ENERGY TRANSFER AT THE CONVECTION BOUNDARY

R. C. Olsen
Department of Physics; Naval Postgraduate School
Monterey, Ca 93943

J. L. Roeder
Aerospace Corp.
El Segundo, Ca

Submitted to The Journal of Geophysical Research
June 15, 1992;
revised August 17, 1993

ABSTRACT

Measurements near geosynchronous orbit, made during the transit from the plasmasphere to the plasma sheet, show evidence of energy transfer from the ring current ions into the low energy plasma of the outer plasmasphere. The energy density (nkT) of the core (E < 100 eV) electron distribution increases to a level of over 1 keV/cm^3, with about 20% as much energy in the core ion distribution. The ring current ions show an energy density of over 20 keV/cm^3 in the same region, and appear to be the energy source for the enhanced energy content of the plasmaspheric electrons and ions. The electron pitch angle distribution indicates parallel electron temperatures as much as an order of magnitude greater than the perpendicular temperatures, and are consistent with an electron distribution which is initially heated in the parallel direction, and then relaxes in anisotropy. The wave data are consistent with the electron heating being caused by Landau damping of a small $E_{||}$ component in electrostatic ion cyclotron waves.

Introduction

The region where the plasma sheet approaches the plasmasphere, known as the plasmapause, is a region of dynamic balance between a hot, tenuous plasma (several keV, 1 /cm^3), and a cold dense plasma (0.5 - 2.0 eV temperature, 100 /cm^3 density). Numerous dynamic interactions exist which empty and fill the magnetic flux tubes outside L = 3 [Horwitz, et al 1984; Singh, 1988]. The nature and evolution of these structures is important to understand because they affect processes such as the precipitation of ring current particles (ions) into the ionosphere, and precipitation of plasma sheet electrons.

Study of these processes revolves around the study of wave-particle interactions, which typically involve plasma heating. Most of the existing work has focused on the heating of ions. In turn, most of these studies of ion behavior are concerned primarily with the refilling stages of plasmasphere evolution, and the processes which are observed in the outer plasmasphere. In the work presented here, by contrast, the observations come in the region where the plasmasphere and plasma sheet interact, and are primarily focused on the heating of the thermal electrons.

Thermal Plasma Observations

The interactions which heat the thermal plasma have been a topic of intense interest beginning with the surveys of the ATS-6 electrostatic analyzer data. Surveys of the temperature characteristics of the thermal plasma by Lennartsson and Reasoner [1978] showed that intense fluxes of low energy ions ($n > 10$ ion/cm^3, kT = 1-30 eV) were routinely found in the dusk sector during magnetically quiet times. (The ATS-6 electron data were not addressed during this survey, at least partly because of the abundance of charging effects which perturbed the electron data.) The pitch angle distributions of the ion distributions observed on ATS-6 were analyzed as well [Horwitz and Chappell, 1979; Comfort and Horwitz, 1981]. In particular, observations of "pancake" distributions peaked at 90° pitch angle were commonly found in the dusk sector. These distributions were considered to be important as possible intermediate stages in the filling of the outer plasmasphere; that is, these distributions were thought to be scattered (trapped) ionospheric ions that would eventually evolve to become the plasmasphere ions.

A special class of the 'pancake" ion distributions noted above are the equatorially trapped plasmas [Olsen, 1981]. Studies of equatorially trapped ions (those mirroring within 10° of the equator) utilizing DE-1 and SCATHA data showed that they could be described as bi-Maxwellian distributions, with perpendicular temperatures an order of magnitude (or more) greater than the parallel temperature [Olsen et al, 1987; Scott, 1991]. These ions are considered to be either ionospheric flows or plasmaspheric ions that have been transversely accelerated (heated). These heating processes appear to be associated with ion Bernstein waves, also termed equatorial noise [Russell et al, 1970; Gurnett, 1976; Perraut et al, 1982]. This process is felt to derive energy from ring current ions.

Reports of preferential heating of He+ by Young et al [1981] in the presence of ion cyclotron waves stimulated enormous interest in the theoretical community [Roux et al, 1982]. One of the early successes of numerical simulation was the matching of simulation to the GEOS results by Omura et al [1985]. The energy source for this heating was considered to be the anisotropic energy distribution of the ring current ions. Hence, this is an example of the transfer of energy from the ring current to the plasmasphere.

The link between the plasma sheet and the processes which fill (refill) the outer plasmasphere are hinted at by GEOS-2 Supra thermal Plasma Analyzer (SPA) data. The outer plasmasphere was found to be a region where field-aligned ion streams were found when the ambient plasma density was in the 30-50 ions/cm^3 range [Sojka et al, 1984]. These ion distributions were found to occur concurrently with relatively dense, warm electron populations measured over the instrument's normal 50- to 509-eV energy range, e.g. the inner edge of the plasma sheet. It was suggested that these electrons were an energy source for the formation of the more isotropic, warm ion distributions which eventually form the outer zone of the plasmasphere [Sojka and Wrenn, 1985]

Electron temperature measurements are relatively rare in the plasmapause region, primarily because of the interference caused by satellite generated photoelectrons. This interference is particularly severe in integral flux detectors, such as wide (angular) aperture devices like a retarding potential analyzer (RPA). Reports are relatively scarce since the early work with RPA's, such as the IMP2 instrument [Serbu and Maier, 1966]. IMP2 data showed the now familiar drop-off of density with altitude, and some increase in temperature, up to 1 or 2 eV. Decreau et al [1982] applied the GEOS-1 mutual impedance robe to measurements from L = 4-8, and were able to obtain meaningful results as long as the plasma was well described as a single Maxwellian distribution. Temperatures from 5,000 to 100,000 °K were found in the core plasma.

Details of the pitch angle distributions for the low energy electrons began to appear with the IMP 6 measurements of low energy electrons in the magnetosphere (8-33 RE) [Hada et al, 1981] Observations

were made of bi-directional, field-aligned pitch angle distributions. These observations, over the instrument range of 13.3 eV to 18.1 keV, apparently included the narrow auroral features seen on ATS-6 [Mcllwain, 1975]. There were also, however, highly anisotropic distributions at lower energies. The first example of Hada et al shows substantial anisotropy down to 103 eV, and fits to the distribution function indicate a parallel temperature of 85 eV, and a perpendicular temperature of 45 eV, at a density of 0.44/cm^3. These observations were made at ~22 RE, and hence presumably not directly related to the plasmapause region observations reported below, but there are some intriguing similarities, as will be shown.

Particle measurements from GEOS-2 made by the suprathermal plasma analyzer (SPA) offered one of the best opportunities to characterize the thermal electrons with differential measurements down below 1 eV. Unfortunately, instrument peculiarities ultimately prevented routine analysis of the electron data below 50 eV [Johnson et al 1978]. One major result which did arise from the GEOS-2 data was the initial report of equatorially trapped electron distributions. The GEOS observations were in the morning (6-12 LT) sector, within a few degrees of the magnetic equator. These distributions of 50-500 eV electrons were anti-correlated with dense, cold plasma (e.g. the plasmasphere) as encountered by GEOS-2 in the afternoon sector, and positively correlated with intense electrostatic emissions, the n + f_{ce} waves [Gough et al, 1979; Wrenn et al 1979]. Electron data from the electrostatic analyzers on SCATHA showed similar trends [Olsen; 1981]. As with the equatorially trapped ion distributions, these electron observations can be described as bi-Maxwellians; that is, the energy and angle distributions can largely be reproduced by taking a perpendicular temperature about ten times the parallel temperature, with a common density of 10 /cm^3.

Acceleration of electrons parallel to the magnetic field by ion cyclotron waves was noted by Mauk and McPherson [1980], and by Norris et al [1983], looking at ATS-6 and GEOS data, respectively. Mauk and McPherron seemingly observed phase-bunching of the electrons (their figure 5), that is a collective motion along the magnetic field line induced by the waves, rather than heating. Norris et al show enhancements in the low energy (e.g. 17 eV) electron flux, which could be described as the effect of an increase in the parallel temperature of the thermal plasma. These dayside (noon) measurements were outside the plasmasphere. They note that the presence of ion cyclotron waves corresponded to the appearance of field-aligned electrons except when the cold plasma density was high. These latter measurements might, however, have been of ionospheric photoelectrons, as later reported from this instrument by Coates et al [1985]

The purpose of this work is to look at the thermal plasma at the outer edge of the plasmapause region, and the interactions between the plasmasphere and plasma sheet populations. This analysis will show that the electrons resident in the outer plasmasphere are anisotropic, with parallel temperatures substantially greater than their perpendicular temperatures. These electrons are seen at the same time as low-frequency electrostatic waves, which could mediate a transfer of energy from the high energy (1-10 keV) ions to the plasmaspheric background

Satellite and Instruments

The Air Force P78-2 satellite was launched on January 30, 1979, as part of the joint NASA/Air Force program on Spacecraft Charging at High Altitudes (SCATHA). The satellite was placed in a near geosynchronous orbit, at 7.9° inclination, 5.3 RE perigee, and 7.8 RE apogee. The satellite was spin stabilized, with a rotational period of about 59 seconds. The spin axis was oriented perpendicular to the earth-sun line, roughly in the orbital plane. Hence, at local midnight, the spin axis is pointing east. The cylindrically shaped satellite measured roughly 1.7 meters in diameter, and 1.75 meters in length. The surface is made up of both insulated and conducting materials. The sides are primarily insulating solar cell glass covers. The satellite was instrumented with an abundance of instruments designed to observe charging effects [McPherson et al, 1975].

The instruments of interest for the work presented here were the UCSD plasma analyzers (SC9), the Aerospace plasma analyzers (SC2), the Lockheed mass spectrometer (SC8), and the GSFC electric and magnetic field detectors (SC10 and SC11). Fennell [1982] described the satellite and instruments, as did Olsen and Norwood [1991].

The SC9 electrostatic analyzers were packaged into two pairs of rotating detectors, each measuring ions and electrons, and a fifth detector fixed viewing radially from the satellite. During both of the time periods studied below, the high energy (HI) rotating detector was parked viewing roughly parallel to the spin axis, measuring particles with energies from a few eV up to 81 keV in 64 logarithmically spaced steps. The low energy (LO) rotating detector was sweeping in angle, as it measured ions from ~2 eV to 1800 eV, and electrons from 20 eV to 1800 keV. The data from the fixed ion detector are not used, here. Energy resolution is ~20%, angular resolution is 5°x7°. [Olsen and Norwood, 1991]

The SC2 detectors are also electrostatic analyzers, covering a somewhat more limited energy range, and operated so as to consistently obtain good angular coverage. The subset of the SC2 data used here come from a detector viewing radially from the satellite body, providing angular coverage which is highly complementary to the SC9 data. [Fennell, 1982]

The ion mass spectrometer (SC8) provided mass and energy analysis of the 100-eV to 32 keV ions. The data are accumulated over fairly long intervals, as the instrument cycles through energy, angle, and mass. Data shown below are averaged in pitch angle, and accumulated over a 30 minute period. Quinn and Johnson [1985] illustrate the capabilities of the instrument, and the nature of the H+ and O+ ion distributions encountered at the plasma sheet boundary, as addressed below.

The SC10 electric field instrument is a 100 m tip-to-tip electric field antenna, with outputs provided through filters which cover the 0.1-1 Hz, 1-2 Hz, 2-20 Hz, and 20-200 Hz frequency range. Data from the highest frequency channel have been shown by Olsen [1981]. The magnetometer (SC11) provides the static magnetic field data, and outputs through the same 4 filter bands. The lower frequency bands include the O+, He+ and the H+ gyrofrequency, while the highest range covers the lower hybrid and ion Bernstein range.

Convection, Drift, and Injections

During most orbits of geosynchronous satellites, the satellite will encounter the plasma sheet in the dusk-midnight region, as it leaves the outer plasmasphere (dusk bulge). The evolution of plasmas observed by the satellite can often be interpreted as the result of satellite motion through the boundaries defined by convection [Mcllwain, 1972; DeForest and Mcllwain, 1971; Kivelson et al, 1979; Mcllwain and Whipple, 1986]. One theoretical approach to define the plasmapause, under this paradigm, is that the plasmapause is the last closed drift path (~corotating).

Even in the quasi-static scenario just described, the existence of ~instantaneous injections of hot plasma is required to explain the observed plasmas. ATS-5 and ATS-6 often showed evidence of hot-plasma injections that appeared to be dispersionless - evidence that they were occurring locally. It is not necessary, at this point, to further develop the spatial/temporal arguments that constantly arise out of attempts to describe injections of hot plasma using data from just one satellite. Clearly, the magnetosphere undergoes purely temporal changes, and there are satellite data that are most clearly interpreted in this light [Greenspan et al, 1985]. It is also clear that convection and drift occur.

The work presented below is developed assuming there is a reasonably static structure, through which the satellite moves. The observations could, in general, also be largely described as a sequence of purely temporal variations, without substantial changes in the interpretation.

Finally, since the cold, or core plasma of the plasmasphere is not well observed on SCATHA, the identification of satellite location with respect to the plasmapause is more properly the indication that the satellite is inside the zero energy Alfven boundary, and little or no keV (plasma sheet) electron flux is apparent.

Observations

Routine analysis of the data from ATS-6 and SCATHA showed that on occasion, there would be intense fluxes of low energy plasma that occurred for a few minutes at the spatial/temporal boundary associated with the plasmapause. One particularly good example has been selected for detailed study, with a second example considered more briefly.

Overview - Day 95

Plate 1 illustrates the data that were selected for detailed analysis. This figure is a spectrogram for ions and electrons from a few eV to 81 keV (vertical axes), as a function of time (horizontal axis), utilizing a color scale which plots low count rates as purple/dark blue, high count rates as red. The top panel shows the electron data, the bottom panel the ion data. Data are shown for 5 April 1979 (day 95), for a two hour period beginning at 0900 UT (1730 LT). The satellite is rising from perigee, moving from 5.3 RE to 5.5 RE over this period, at magnetic latitude that ranges from -11° to -13°. The satellite encounters the plasma sheet at about 1020 UT, as indicated by the high fluxes of 1-10 keV electrons (yellow/orange shading). From about 0950-1020 UT, very high fluxes of lower energy electrons (0-100 eV) are found. High ion fluxes are also found at low energy, just prior to the injection. The red band across the bottom of the electron panel is due to the high flux of locally generated photoelectrons, trapped in the sheath near the spacecraft. They extend up to a few eV in energy. The line plot in the center of the plate shows the pitch angle of the measured particles. This angle is initially near 70°, but drops to near 20° as the magnetic field becomes severely distorted.

A review of the geomagnetic indices shows there was a large storm (Dst = -200 gamma) on day 93. The ring current recovered quickly, however, and the Dst plot shows normal conditions at this time. The solar wind, however, showed evidence of a shock, with enhanced magnetic field strength (double), density (~5 times), and flow speed (~50%) beginning early on day 95 [NSSDC, OMNI database]. This increase in solar wind pressure was sufficient to press the magnetosheath inward to geosynchronous orbit on the dayside, as reported by GEOS-2 (G. Wrenn, private communication, 1985).

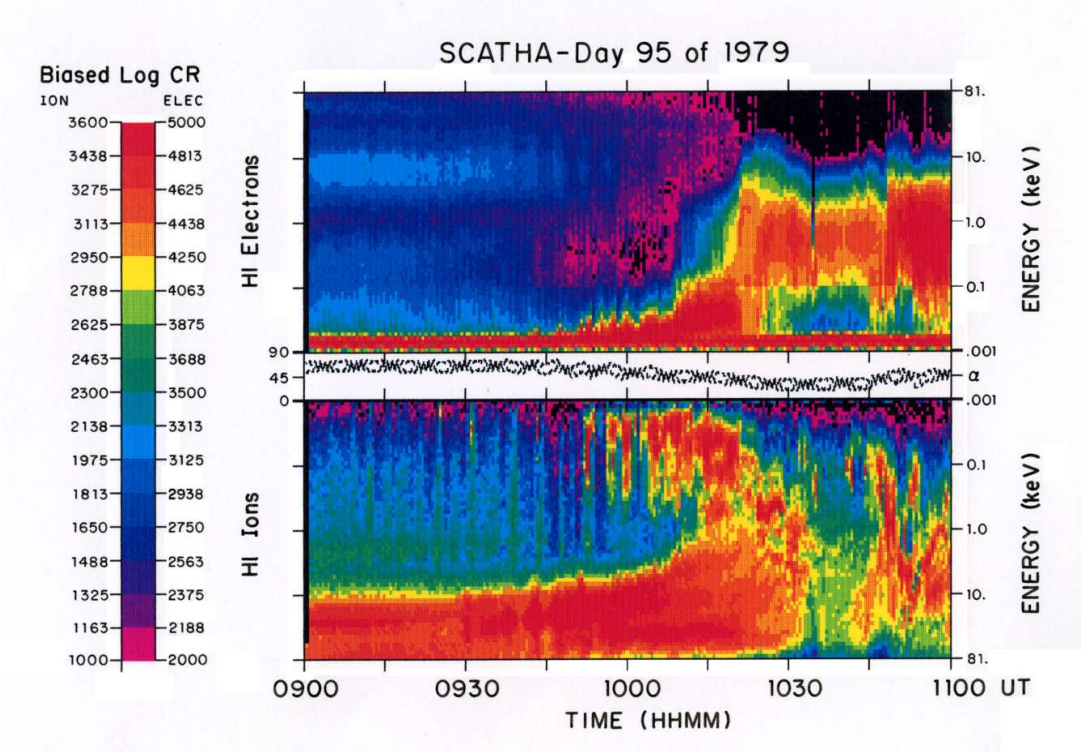

Plate A. Energy time spectrogram for 1 eV to 81 keV electrons and ions. The display uses a biased log to display the count rate.

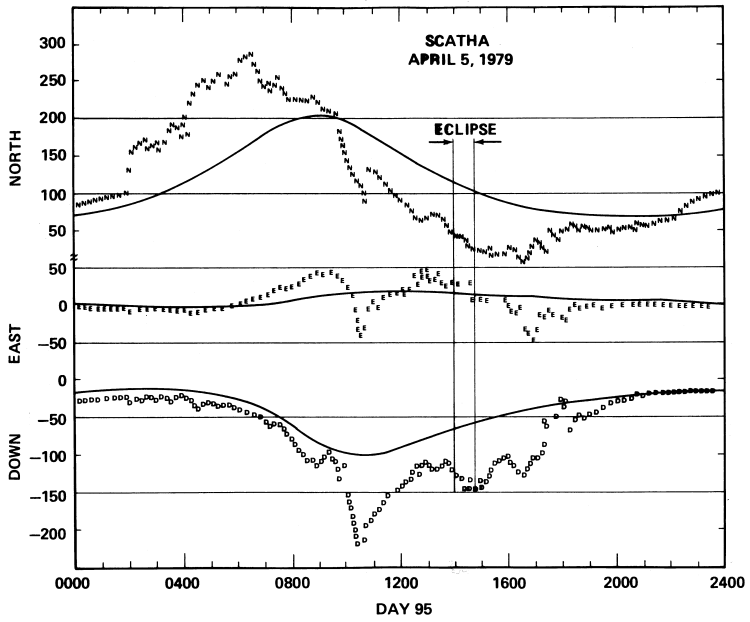

Figure 1. Magnetic fields as observed at SCATHA for April 5, 1979.

The pressure from the solar wind led to a highly distorted magnetosphere, and a substorm, as illustrated in Figure 1. The data are plotted in topographic coordinates (North, East, and Down). The thin solid lines are for a model dipole field, the data are plotted as letters (N, E, and D). The substorm centered just past 1000 UT is apparent. The effects of the substorm are reflected in the plasma behavior shown in Plate 1.

The result is that the satellite encounters a region of heated thermal plasma, as partly illustrated above. The point is made more clearly by converting the plasma data from flux (count rate) to distribution function (or phase space density). Plate 2 shows the data from the high-energy detector. The approach is similar to that used in Plate 1, but with the color scale cycling at the midpoint. This cycling is necessary because of the relatively large dynamic range produced by the conversion to distribution function. The detector is parked viewing parallel to the spin axis (approximately radially inward at local dusk).

Beginning at 1000 UT, the 1-100 eV electron distribution rises out of the local photoelectron cloud (bottom few channels in plot). This is represented by the red region in plate 2, below 100 eV. A similar increase is found in the ions, with a bright red region at low energies. In addition, the presentation of the data in this format allows the local maximum in the ion distribution function at ~10 keV to show up. This maximum is apparent from 0930-1010 UT. This pattern is also evident in the count rate (Plate 1), but it now becomes clear that the peak in flux is also a local maximum in phase space density.

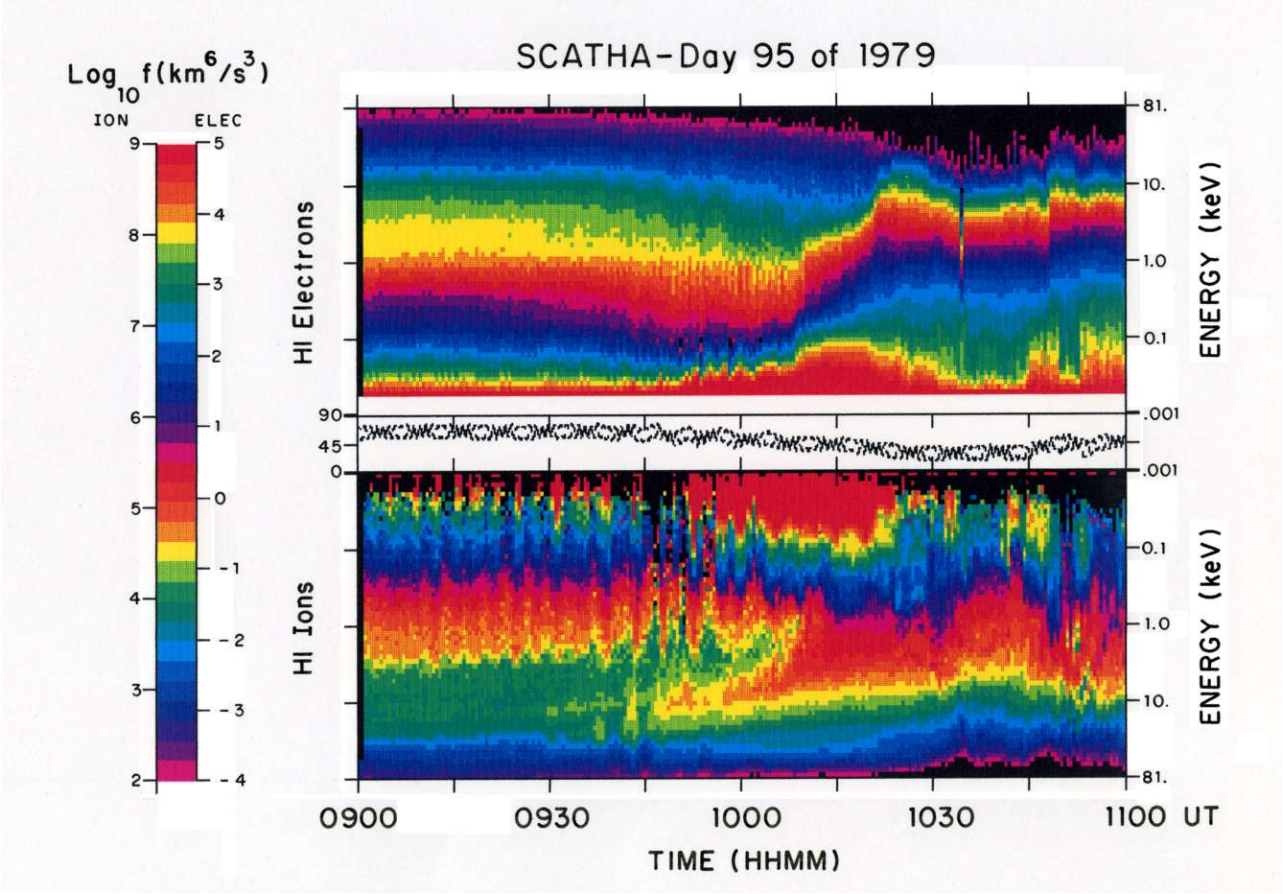

Plate B. Electron and ion distribution functions.

Energy Analysis - Day 95

The thermal plasma data were summarized by considering both least-square-fits of the distribution function, and by calculating moments of the distribution functions. These techniques are appropriate if the distributions are approximately Maxwellian. This is reasonably true for the electron data during this period; less so for the ions. The ion data show a flat distribution at low energies, which is symptomatic of quasi-linear diffusion (compare distribution functions shown by Olsen [1981]). Density, temperature, and pressure or energy density (nkT) were calculated.

Figure 2 shows the results analysis of the electron data from 10-100 eV, Figure 3 shows the results from the analysis of the ion data (1-100 eV). The upper limit for the 'thermal' plasma was arbitrarily set at 100 eV, as a useful and convenient breakpoint. The lower limit for the electron moments was determined by the need to exclude the local photoelectron cloud from the calculations. No correction for spacecraft potential effects has been made at this point.

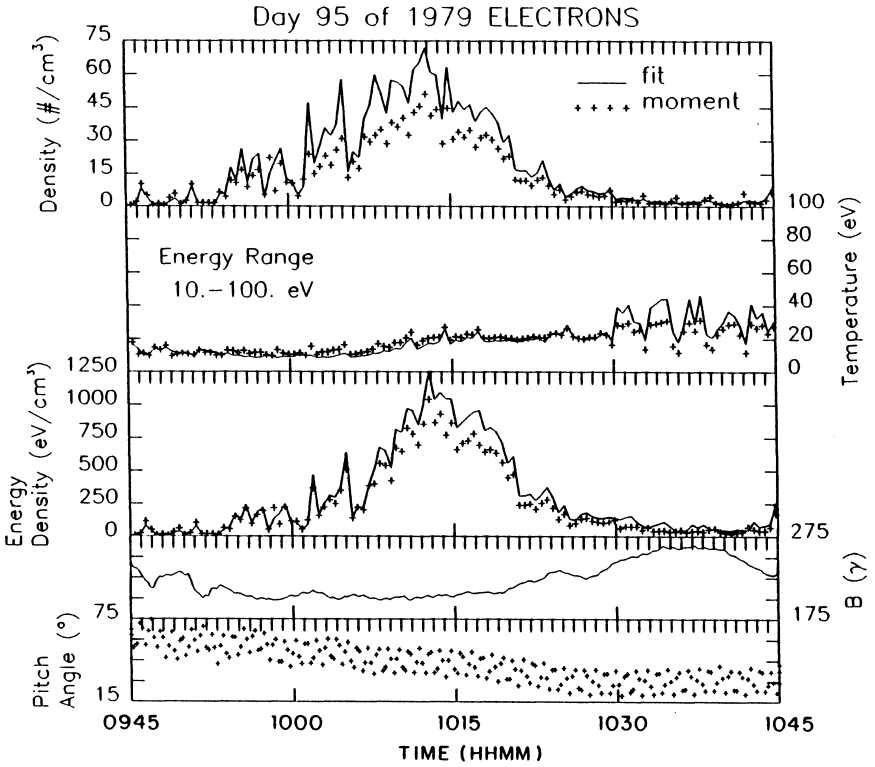

Figure 2. Electron plasma parameters.

The primary correction that would be useful to make is to somehow account for the unmeasured particles, particularly the 'hidden' ions [Olsen, 1982]. This is difficult to do. This becomes less important as the temperature increases, and the ions acquire enough energy to overcome the charging barrier. The other correction which ought to be made is the exp(q 4/k T) term which modifies the observed portion of the distribution function. Here, the potential, 4), is of the order 1-5 V. For the observed portion of the distribution function, this correction is not large, because kT is high. The relative importance of these effects can be assessed by comparing the calculated ion and electron densities. Figures 2 and 3 show reasonable

agreement in density at 1015 UT, as the energy density peaks. This indicates that the errors due to charging and unmeasured portions of the distribution function are not large at this point. Agreement between the least-square fit and moment calculations gives a similar reassurance. The other major concern regarding the validity of these calculations is the effect of anisotropies in the particle distributions. These are partially observed, but again cannot be easily accounted for.

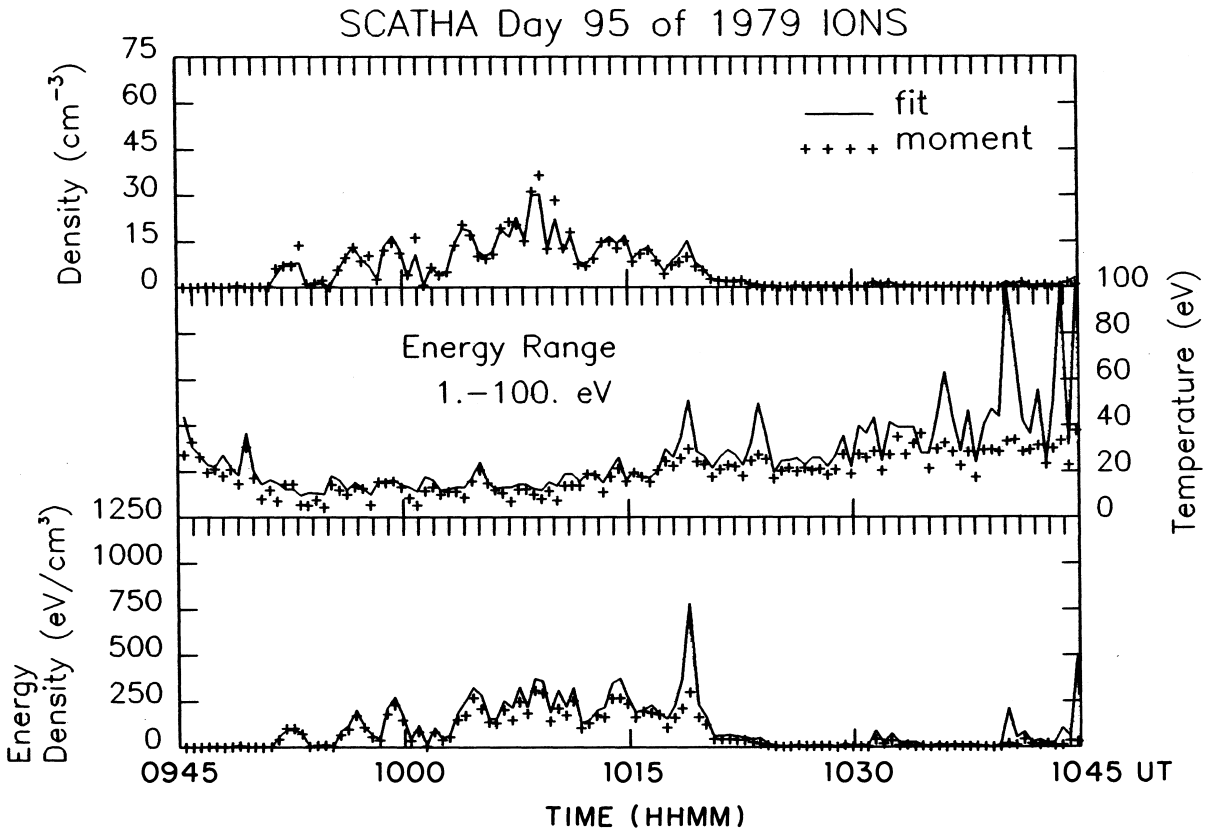

Figure 3. Ion plasma parameters

Figures 2 and 3 show that the observed portion of the ambient plasma distribution increases significantly in density, temperature, and energy density, with the peaks at 1015 UT. The density calculations show peak values of 30 ions/cm^3, or 60 electrons/cm^3. This is reasonably good agreement, though it appears that some portions of the low energy ion distribution remain unmeasured. The temperature of the electrons roughly doubles, from 10-20 eV. The ions behave in a similar fashion. The energy densities show the most obvious increase, and the electron energy density approaches a keV/cm^3. The thermal plasma has acquired an energy density comparable to that found in the plasma sheet. The pitch angle range for the observed particles is plotted in the bottom panel. Two things can be learned from this. First, there is a substantial fluctuation in the pitch angle range associated with these observations, of about 20° during a given energy sweep. This is due to the fluctuations in the magnetic field direction. Second, the center of observed range varies over this period. This will affect the values calculated for n, T, and nkT, since the electron distribution is highly anisotropic. This is probably the largest source of error in the attempt to characterize the electron distributions. The total magnetic field is included for reference purposes. The substorm is less obvious in the total field, than in the components, which were shown in Figure 1.

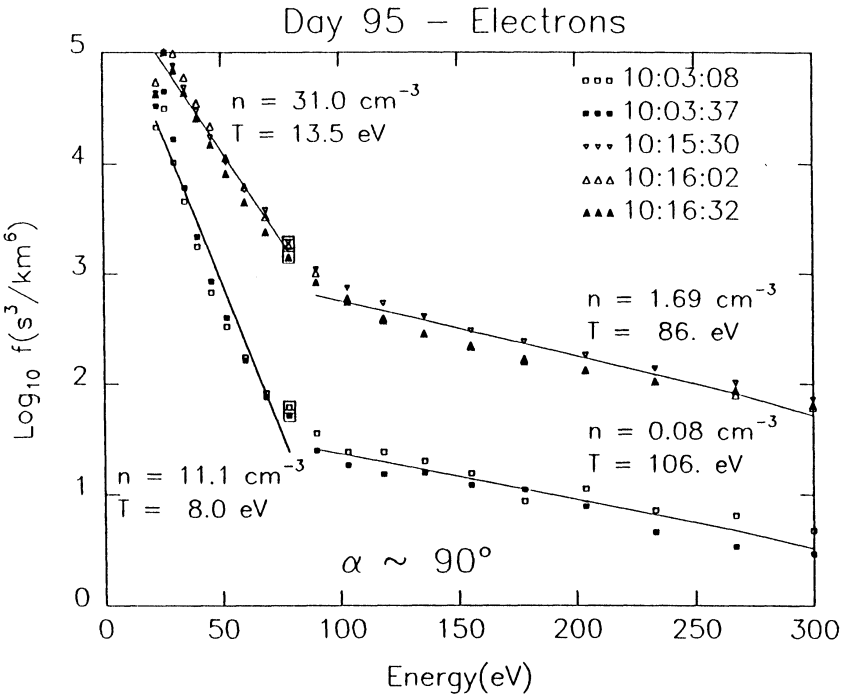

Figure 4. Electron distribution function.

Data from the LO electron detector, during periods of measurement along the 90° direction, give some of the details of the electron energy distributions. Figure 4 shows the electron data with piece-wise least-square-fits. Data taken at 1003 show the initial enhancements in energy (and apparent density) as the satellite leaves the plasmasphere proper. Data taken at the location of the highest energy density (1015 UT) show that two characteristic slopes describe the electron distribution, with the core of the plasma heated to a temperature of over 10 eV. (The lack of data below ~20 eV, due to a detector operation mode, hides a portion of the electron spectrum. This portion of the spectrum contributes a significant amount to the HI detector density values plotted in Figure 2.)

The higher energy (>100 eV) portion of the electron and ion distribution functions was considered to see just how much energy was available. Figure 5 shows the electron and ion data. In the electron data (solid lines), only a faint remnant of old plasma sheet electrons is found prior to 1008 UT (peaking at 10 keV in flux in plate 1). This plasma is characterized by a density of about 0.1 electron/cm^3, and a kinetic temperature of 4-5 keV. (Fitted values do not seem appropriate over an energy range where the distribution is clearly not Maxwellian.) Following the injection of hot plasma, the apparent temperature drops to about 500 eV, reflecting the large contribution of lower energy electrons to the moment calculation. (Restricting the range of integration to 1 keV to 80 keV causes the estimate for the electron density to drop by a factor of 2-3, with an increase in temperature of a factor of 3.)

The electron energy density is initially about 0.5 keV/cm^3. Following the passage into the plasma sheet, and subsequent injection, this increases by an order of magnitude. Clearly the pre-existing hot plasma did not have sufficient energy to heat the plasmasphere electrons, but the hot plasma injected at 1020 did. The heating, of course, precedes this time. It would appear that the energization process is not a result of a direct coupling, but may perhaps be a result of the injection process.

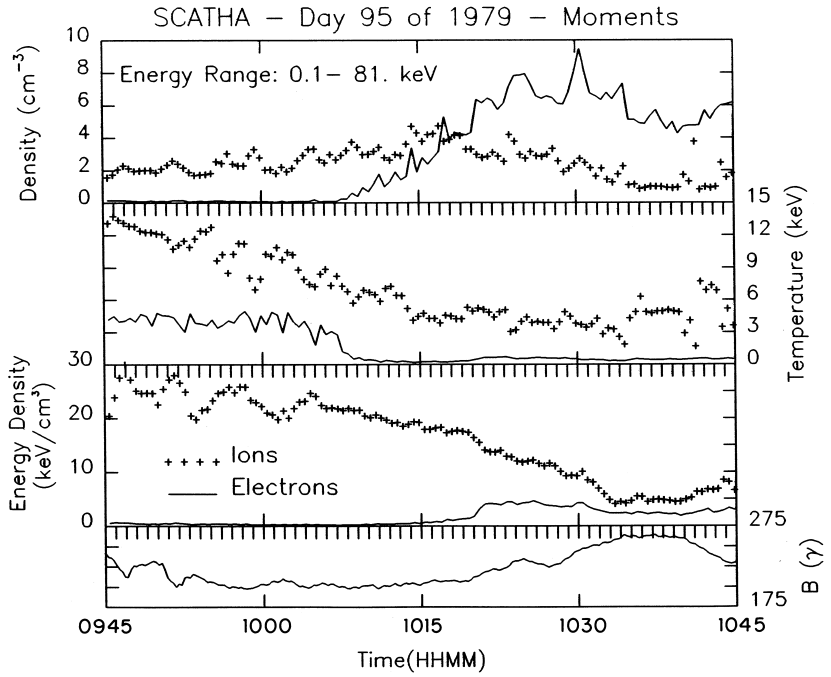

Figure 5. Hot plasma parameters.

The ion energy density is substantially higher. The ions have enough energy to produce the ~1 keV/cm^3 (electron and ion) thermal distribution found at 1015 UT from 0-100 eV. Simple energy arguments, along with the distribution function shape, therefore suggest that the ring current ions are the energy source for the observed heated plasma.

Angular Distributions - Day 95

The nature of the plasma interactions occurring here depends on a knowledge of the evolution of the angular distributions, particularly for the electrons. This was obtained using the SC2 detectors, and the SC9 LO detector. Several unexpected results occurred. Previous experience with heating suggested that the heated plasma would be heated in the perpendicular direction. The energetic particles are normally expected to be fairly anisotropic. Neither proved to be true.

Angular distributions take one spin of the satellite to acquire with the SC2 detector, or one minute. Data taken at 87 and 187 eV (the two lowest energy channels) are used here. The angular distributions available from the SC9 detector are less regularly spaced, due to the coupled angular rotation, satellite spin, and energy dwell patter. Angular distributions from the SC9 experiment are available at 8.4, 26, 78, and 233 eV.

Plate 3 illustrates the evolution of the angular distribution of the 87 eV electrons. As in the previous plates, the data are presented in spectrogram form, for a 2-hour interval. The color-coding scheme is the same as in plate 1, but the color scale is a simple log scale. The black regions in Plate 3 reflect the lack of measurements along the magnetic field line - a problem that becomes increasingly acute after 1005.

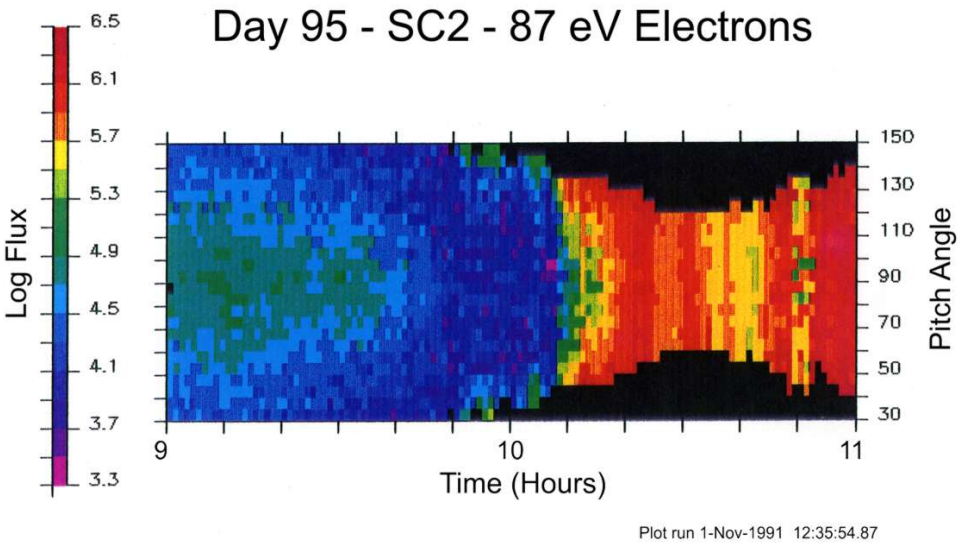

Plate C. Electron pitch angle distributions.

Early in the time period illustrated in plate 3, the electron distribution shows a modest peak at 90° pitch angle. Beginning at 1000 UT, enhancements being to appear in the field-aligned bins. The enhancement in the field-aligned plasma is most evident from 1010-102 UT. At 1020 UT, the distribution relaxes to an isotropic distribution, over the observed pitch angle range.

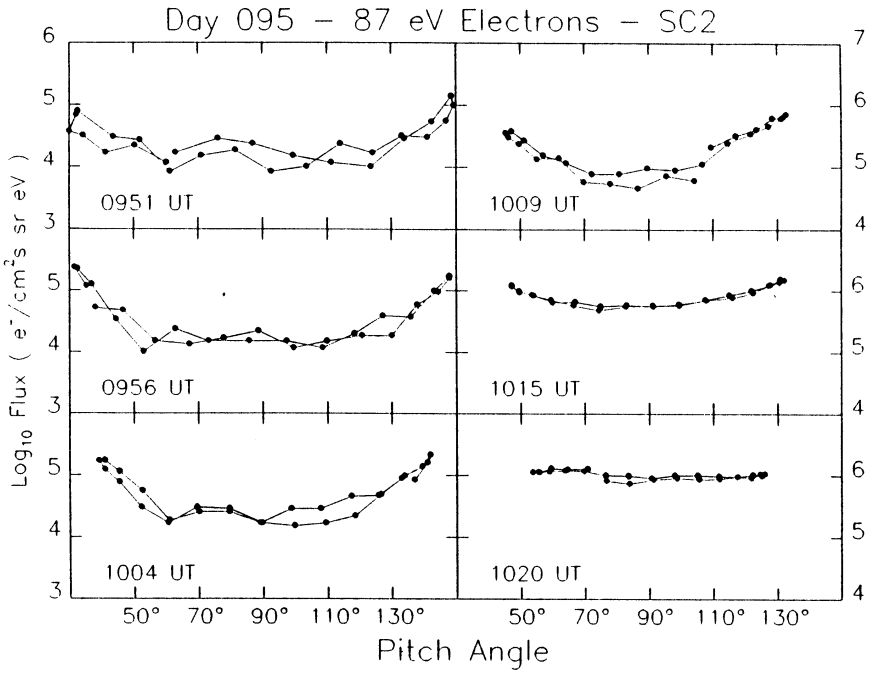

Figure 6. Pitch angle distributions

Figures 6 and 7 show the evolution of the plasma pitch angle distributions in line plot form. Figure 6 shows the 87 eV electron data (as in Plate 3) for a few selected times. The pitch angle range is effectively swept twice during a spin, hence the dual curves in each panel. Some variations due to temporal effects can be seen, but the segments shown here were selected for constancy of the angular distribution over the two half-minute sweeps. The anisotropy over the observed pitch angle range is about an order-of-magnitude at 1004 and 1009 UT, and the curves are almost flat by 1020 UT.

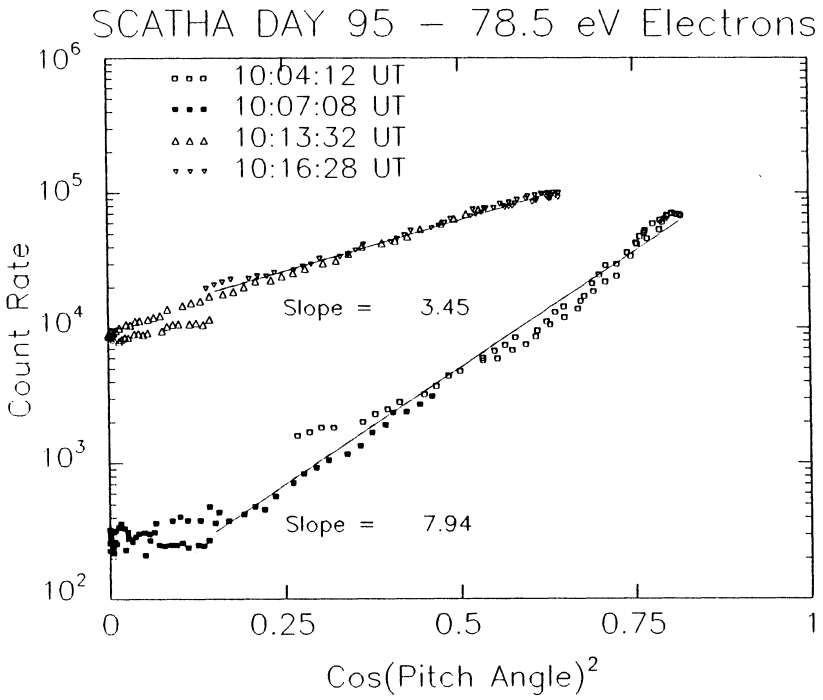

Figure 7. Electron pitch angle distribution.

A different approach is used to show the more detailed electron angular distributions from the SC9 instrument. The heated plasma distributions observed previously on SCATHA [e.g. Olsen, 1981] can partially be described as bi-Maxwellians, that is distributions with different parallel and perpendicular temperatures. It can be shown that for a bi-Maxwellian, a plot of the angular distribution of the flux, or distribution function, vs. $\sin^2\alpha$ or $\cos^2\alpha$ will be a straight line. The slope of this line depends on the ratio of the parallel and perpendicular temperatures. If one is known (in our case, the perpendicular temperature), the other can be obtained. Since measurements along the field line are difficult to obtain, this is a powerful technique in obtaining characteristic values for the field-aligned plasma..

Figure 7 shows the SC9 data at 78 eV, which are close in energy to the SC2 data shown in Figure 6. Four angular distributions are available at this energy. They are all well ordered by this approach to plotting the data. The data taken at 1005 show the highest degree of anisotropy. The distribution is well represented as a bi-Maxwellian from ~60° down to ~25°. During the period of peak T_{perp}, ~1015 UT, the distribution is again well described by a bi-Maxwellian over the observed range of pitch angles, from 90° to 35°.

The field-aligned nature of the electron distributions was somewhat surprising, and more or less immediately rules out perpendicular acceleration by, for example, electron cyclotron waves. An analysis of the SC2 data (not shown) indicates that the preferentially field-aligned character of the electron data extends up to 1.9

keV (most clearly found from 1010-1015). The distributions are flat above 2 keV. Curiously, the peak perpendicular temperatures (e.g. Figure 2) follow the period of peak anisotropy. This may indicate an initial heating parallel to the magnetic field, followed by a relaxation in the pitch angle distribution which enhances the perpendicular temperature. (From a spatial point of view, the highest anisotropies are found near the plasmasphere; the higher temperatures tend towards the plasma sheet edge of this region). There is also a subtle variation in when the peak anisotropies are found. The preferentially field-aligned character of the electrons develops first in the lower energy particles, and then appears at higher energies, as described below.

Analysis of the 8.4 eV electron distributions (not shown) revealed they were generally flat throughout this period, with faint indications of an enhancement by a factor of 2 in flux above 160°. The 26 eV electron distributions, from the core of the electron distribution, evolve from a fairly flat distribution at 0945-0950 UT, to a highly anisotropic distribution at 0955 UT, with a slope of 3.8. By 1013 UT, the core of the electron distribution function is relaxing back towards isotropy.

The SC2 data at 187 eV show a similar level of anisotropy, but it occurs later in the sequence, at ~1010. Data taken by SC9 at 233 eV at 1008 UT show an angular distribution very similar to that shown for the 78.5 eV electrons at 1004 and 1007

Slopes fitted to the angular distributions as described above range from 1 to 8, with nominal values of 3-4 most commonly found, as illustrated in Figure 7. Perpendicular temperatures obtained from fits such as those shown in Figure 4, give characteristic temperatures of ~40 eV below the ~75 eV breakpoint, and ~100 eV above that point. Combining the information obtained in these two ways gives a ratio of parallel to perpendicular temperature of ~2. The slope of ~8 found for the 78 eV electrons at ~1005 suggests a ratio of parallel to perpendicular temperature of 10 or more, and hence parallel temperatures of the core electron distribution of several hundred eV. This occurs at a density of over 10 /cm^3.

The ion data (not shown here) were also examined. The 74 and 154 eV (SC2) ion channels appear to show slight enhancements in the field-aligned direction in the 1000-1015 time period, with ~2x higher flux at 35° than at 90°. The 135° flux (away from the equator) is only slightly elevated over the 90° flux. These observations are distorted by the presence of a pulsation, which introduces temporal fluctuations on the same time scale as the pitch angle sampling (~1 minute).

The hot ion pitch angle distributions are flat in the electrostatic analyzer data from 2 keV to 15.6 keV over the observed pitch angle range of 45° to 135°, and in the 19 keV, 36 keV, and 71 keV solid state ion detectors over the same pitch angle range, for the entire period.

Energetic Ions - Day 95

As the last element of the particle data, we examine the nature of the probable energy source, the high-energy ions. Figure 8 shows the ion distribution function, as a function of energy, at 0950, 1000, and 1010 UT. The data from 1000 UT have been multiplied by 10, the data from 1010 UT by 100, in order to separate the traces. The distribution function clearly has a local minimum, as noted previously with Plate 2. At 0950, there is an increasing slope in f from 2-10 keV. The region of positive slope decreases in energy, with time, and only extends to 3 keV at 1010 UT. This minimum is due to magnetospheric convection, and has been named by McIlwain as the "deep proton minimum" [DeForest and McIlwain, 1971; McIlwain, 1972; Fennell et al, 1981]

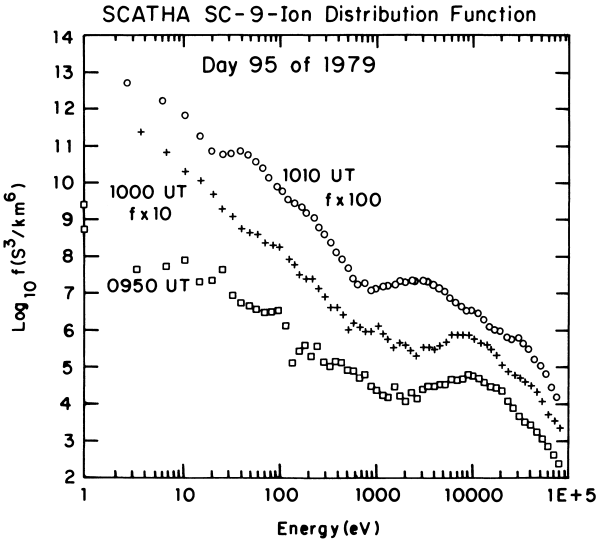

Figure 8. Hot ion distribution function.

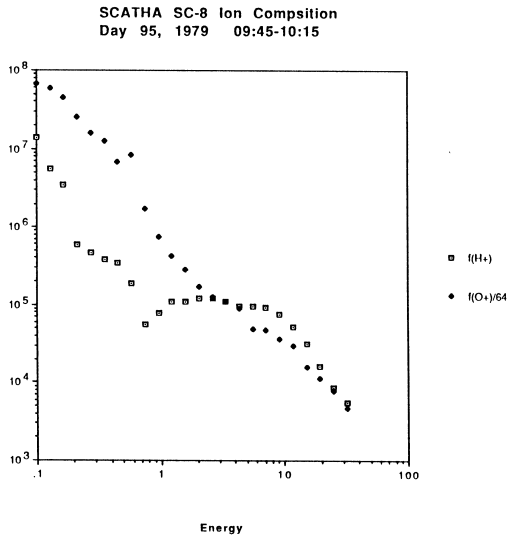

Figure 9. Hot ion distribution function.

The mass composition can be checked by using the mass spectrometer (SC8). Figure 9 shows the pitch-angle averaged data accumulated from 0945-1015 UT. This relatively long interval for accumulation is necessary to develop reasonable statistics. The figure shows that the low energy (100 eV- 2 keV) plasma is largely O+, as is typically found below the ion minimum [Quinn and Johnson, 1985; Kaye et al, 1981]. The minimum in the distribution function is in H+. We must assume that these characteristics of the data are not a function of pitch angle, given an absence of further information.

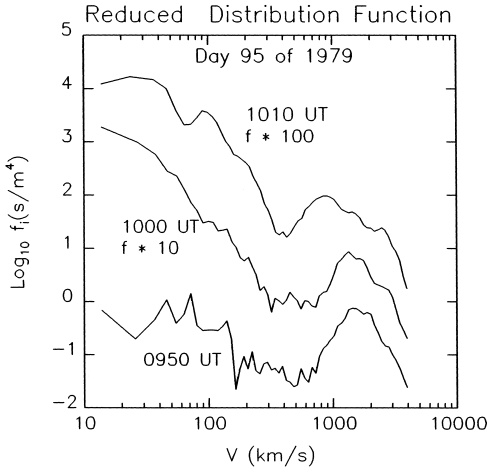

Figure 10. Reduced distribution functions.

Elementary plasma theory requires that the 2 directions transverse to k be integrated out, in order to calculate growth rates. This is difficult to do without a full, 3 dimensional distribution function. The high energy ions appear to be isotropic, however, so spherical symmetry is assumed, and the reduced distribution function is calculated (essentially, $v^2 f(v)$) Again, the distribution function values are obtained from the electrostatic analyzer with the assumption that the ions are protons. With these assumptions in mind, Figure 10 shows the reduced distribution function, as a function of velocity (instead of energy). Note the change in units on the y axis, as well. It can be seen that the reduced distribution function has a minimum in the velocity range of a few hundred kilometers per second, followed by a relatively steep upward slope. The relative importance of O+ below 1 keV, indicated by the mass spectrometer data, means that the proton distribution function would be substantially reduced below a few hundred km/s, accentuating the region of positive slope.

Wave Data - Day 95

The remaining element of the observational data set to consider is the wave data. Two sets of data are available. The plasma wave instrument on SCATHA sampled electric and magnetic field data at 400 Hz, 1.3 kHz, 2.3 kHz, 3.0 kHz, 10.0 kHz, 30 kHz, 100 kHz, and 300 kHz. Contrary to hopes and expectations, there were no signals observed that correlated with the observations of heating. In particular, there was no evidence of enhanced activity near the gyro frequency (or n+'/2) in the 10 kHz channel, and no evidence of enhanced activity near the upper hybrid resonance frequency (30 and 100 kHz channels) [Kurth et al, 1979]. These channels are all broad enough to show such activity if it is occurring.

The electric and magnetic field instruments provided filter data in 4 wide bands: 0.1-1.0 Hz, 1.0-2.0 Hz, 2.0-20. Hz, and 20-200 Hz. The first 3 bands correspond roughly to the ion cyclotron frequencies for O+, He+, and H+ (~3 Hz), respectively. The 20-200 Hz channel corresponds to the geometric mean gyro frequency. This latter channel typically shows a strong response to ion Bernstein mode waves observed near the magnetic equator [Olsen, 1981].

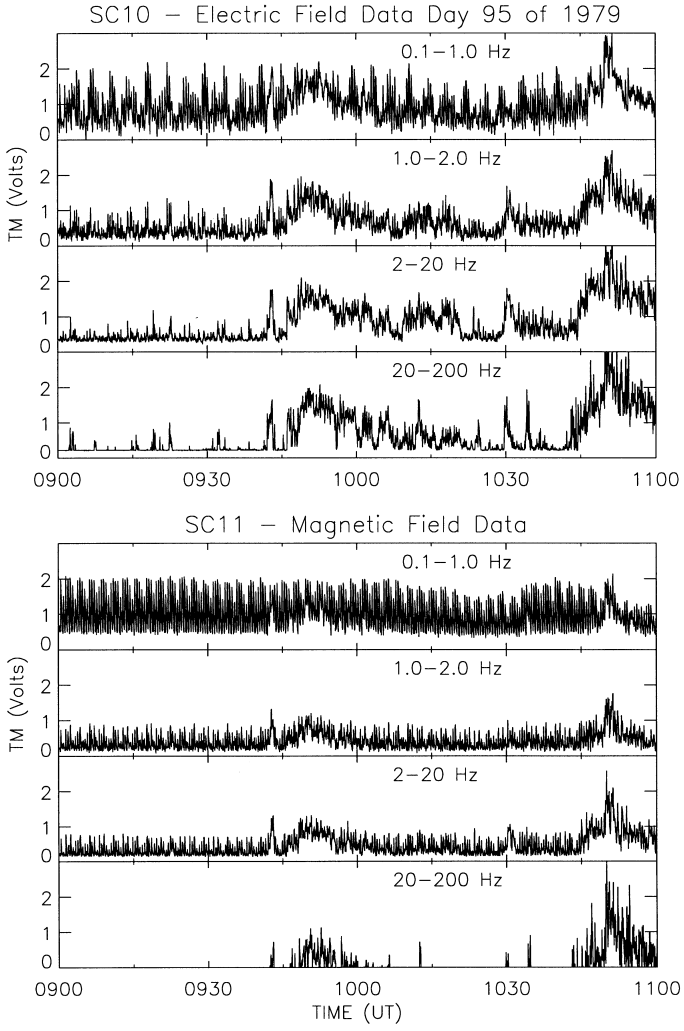

Figure 11. Electric and magnetic field wave amplitudes.

Figure 11a shows the electric field data, Figure 11 b shows the magnetic field data. There is a fairly large signal in both instruments prior to 1000 UT, which is poorly defined, aside from being clearly electromagnetic. The magnetic amplitude is about 0.5 gamma. There is a second electromagnetic disturbance just prior to 1100. Neither of these corresponds temporally to the peak of the observed heating. There is a less obvious, apparently electrostatic signal centered at ~1015 UT, which is strongest in the 2-20 Hz channel.

The signal at 1015 UT has an amplitude of a few tenths of a millivolt per meter. The magnetic signature is near the noise level, and is at or less than 0.05 gamma. For an Alfven wave, the electric field amplitude of ~0.2 mV/m, and an Alfven speed estimated to be ~400 km/s predict a magnetic signal of ~5 gamma (nT), or about 3V on the telemetry scale. The identification of the waves is difficult without more precise spectral information. Analysis of the spin variation of the 2-20 Hz signals indicates that the electric field signal is polarized perpendicular to the magnetic field line. It seems possible that the electric field antenna is responding to electrostatic ion cyclotron waves.

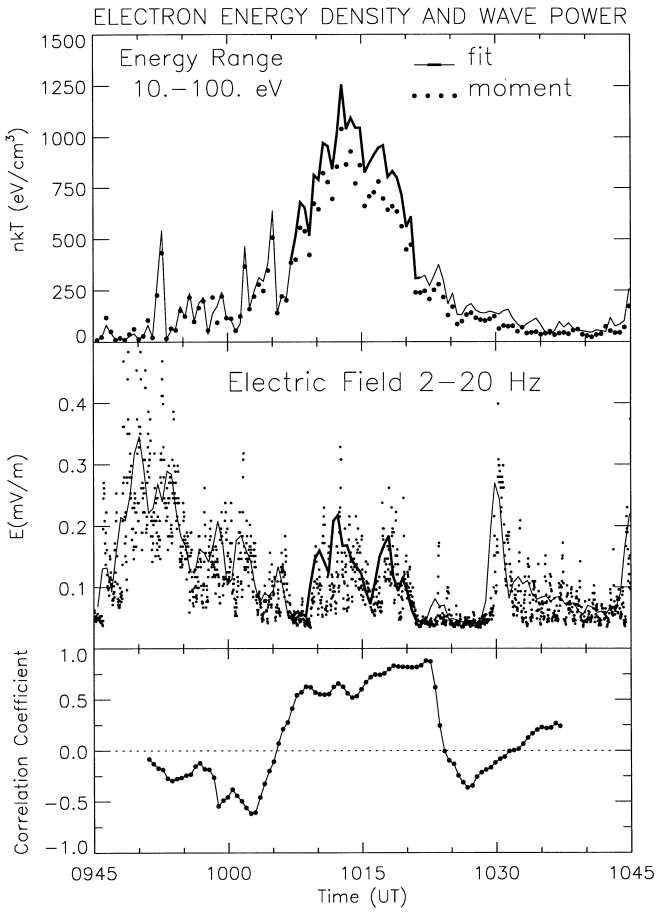

Figure 12. Electron energy density and electric field wave power.

The relationship between the wave power and the heating of the low energy electrons is presented in Figure 12. The top portion of the figure presents the information previously given in Figure 2, for the energy density. The middle panel presents the 2-20 Hz wave data. The spin modulation of the electric field data makes direct use of the data awkward. Therefore, the data were fitted to the sine of the angle the antenna made with the magnetic field, using a sliding 1-minute window (one full spin). The raw data points are then

plotted in Figure 12, along with the fit to the E⊥B value (the solid line). Elements from this fit were then cross-correlated with the energy density obtained from the distribution fits, as presented in the bottom panel. Roughly 11 minute sliding averages are used in the cross-correlation (23 data points). The broadband electromagnetic signal prior to 1000 UT is not obviously related to the appearance of warm, dense plasma, decaying before the energy density increases. The more modest electrostatic peak centered at 1015 is at least temporally coincident with the observations of warm dense plasma.

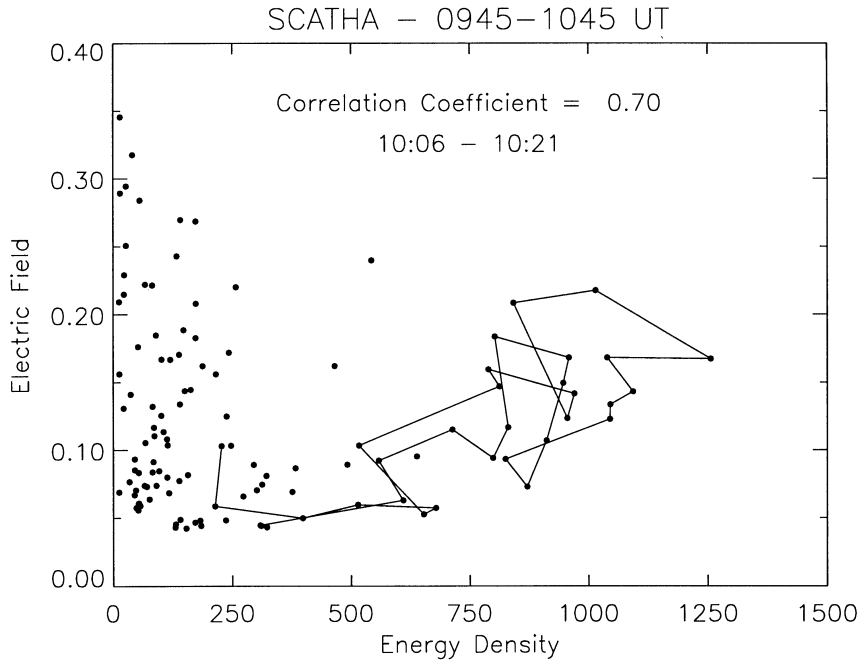

Figure 13.

The correspondence between the two data sets is considered one final time, in figure 13, where the electric field is plotted vs the energy density. The period of the peak energy density, 1006-1021 UT, is emphasized by drawing a line through those data points. This period is also emphasized in figure 12, in the top and middle plots, with a thicker line drawn in both panels. The correlation coefficient for this 14-minute interval is 0.72. This value, while significant, is not conclusive.

Plasma Data - Day 293

The example from day 95 of 1979 is unusual in the intensity of the thermal electron flux observed, and apparently, the amount of heating observed. This raised the electron flux far enough in energy to make it clearly separable from the satellite-generated photoelectron cloud. This day was also unusual in the available range of pitch angle information and mass spectrometer data. A more typical example of the plasmapause transition is presented next.

The second example occurs an hour prior to local midnight, on day 293 of 1979. (The previous example is just past local dusk.). The satellite is within 2° of the magnetic equator, at L = 6.3. Plate 4 illustrates the plasma behavior from 2000-2042 UT. The detector is parked viewing nearly parallel to the spin axis, and is

viewing eastward, at ~90° pitch angle. The satellite leaves the plasmasphere at 2021, and there is a modest injection at 2028 UT. There is again an enhancement in the thermal electron flux.

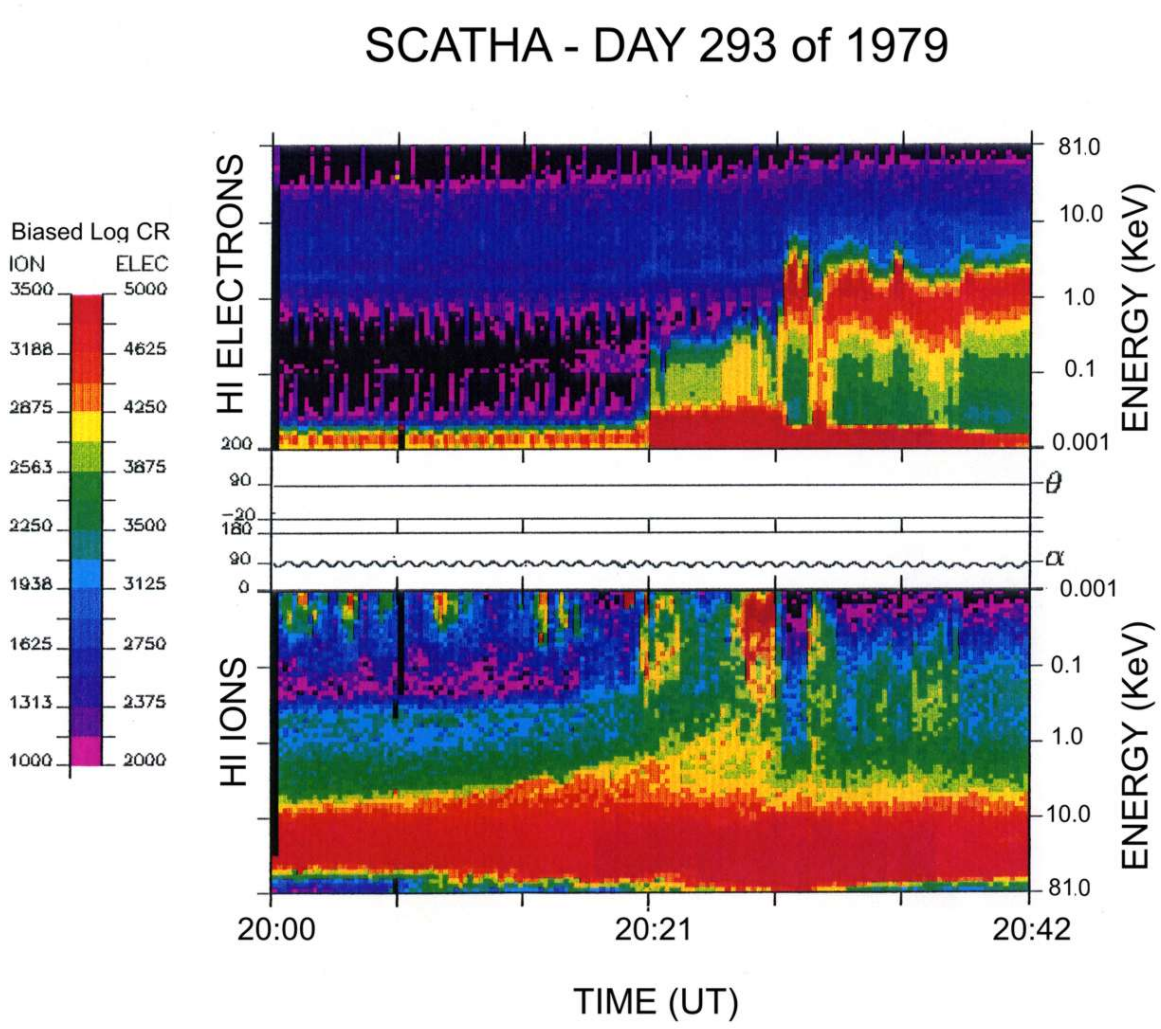

Plate D. Plasma data for day 293.

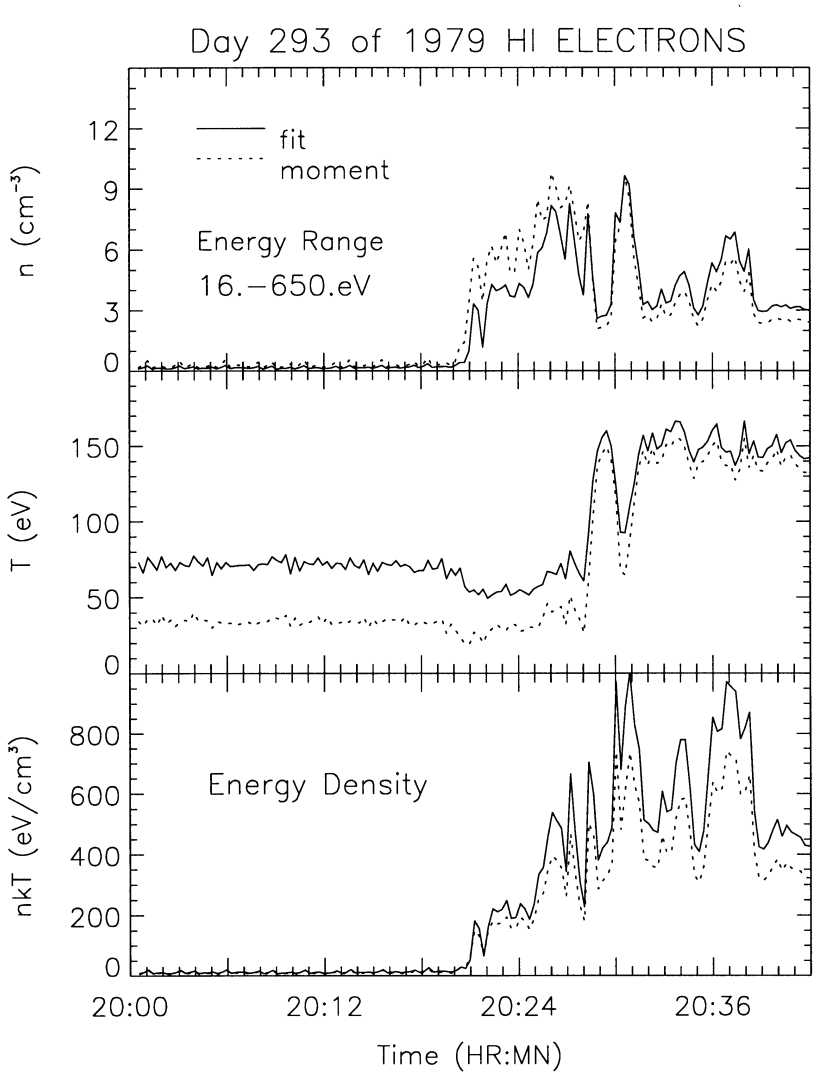

Figure 14 shows the density, temperature, and energy density calculations for this period. The 650 eV upper limit is the upper boundary for the electron population seen from 2000-2028 (Plate 4). Again, the density estimate in the plasmasphere is near zero, because the cold electron background is obscured in the locally generated photoelectron cloud. The satellite potential may be as high as +10 V. The temperature in the early portion of the data is dominated by the remnant drifting echo of earlier injections. The peak in the energy density from 2021 to 2029 is the heated plasmaspheric component. The density dips during the injection, and the warm dense plasma reappears for ~2 minutes following the injection.

All four of the electric field channels are at background for this period. The three magnetic channels from 1-20 Hz show no signal above noise. . There is a reasonably substantial signal from ~2020-2025 UT in the 0.1-1.0 Hz magnetic channel, but the data show evidence of satellite induced artifacts which prohibit further interpretation.

Summary of data

The data shown from days 95 and 293 of 1979 illustrate the passage of a satellite from the plasmasphere into the plasma sheet, in a region of convecting, mixed plasmas. The thermal, or core, plasma appears plasmaspheric in origin, based on the relatively high densities. They could also be of (recent) ionospheric origin, of course. The parallel temperatures inferred for these electrons, of 20 eV or more, indicate that in either case, there has been substantial heating or acceleration of the electrons over the source values. This heating, or acceleration, occurs with a pitch angle distribution that is preferentially field-aligned, at least for the first example, with an electron flux along B that is 1-2 orders of magnitude higher than that found perpendicular to B. It is likely that the energy density of the electron distribution along B has been underestimated.

If the electrons are being heated in situ, he ion portion of the hot plasma distribution must provide the energy for this process, since only the hot ions have sufficient energy density. There is typically a minimum in the ion distribution function for measurements at geosynchronous orbit at a few keV, induced by magnetospheric convection. The region of positive slope reaches a peak at a velocity of about 1000 km/s in the example shown here. The pitch angle distribution of the hot ions appears to be nearly flat in the case shown, which is somewhat unusual..

There is a reasonably large amplitude wave observed in the 2-20 Hz electric field data, with an amplitude of about 0.2 mV/m, on day 95. This is an appropriate frequency range for ion cyclotron waves. The polarization of the wave is transverse to B, which supports that identification. The lack of a magnetic signature may be due to a lack of sensitivity, but seems to indicate an electrostatic mode.

Discussion

One possible explanation for these observations is that the field-aligned electrons are ionospheric in origin, accelerated by low-altitude electric fields into the magnetosphere. Such processes are observed to occur at various energies, from 10-20 eV, to several keV [Laszakovits, 1993; Mcllwain, 1975] If such electrons are the genesis of these observations, the initial acceleration would be followed by a gradual decay in energy and anisotropy much like that found here. Previous experience shows that observations of, distributions peaked in energy (e.g. beam-like) are generally encountered during at least a portion of such obervational sets, and no such distributions were observed at this time. Also, the phase space density generally encountered in obvious cases of ionospheric acceleration are generally lower than those reported here. The same problem comes with any attempt to explain these data as the result of reflection (backscatter) from the ionosphere, as with the work by Moore and Arnoldy [1982]. It also appears that he increasing anisotropy with energy found here also mitigates against explanations of that sort (e.g. Moore and Arnoldy, figure 4).

A second likely interpretation of these data is that ion cyclotron waves are generated by the hot ions. These waves can interact with the low energy ions, according to the pattern previous workers have identified (e.g. Omura et al, 1985; Chen et al, 1988). The thermal electrons can also be heated, primarily through Landau damping. Although the main component of the propagation vector, k, is perpendicular to B, there will in general be some small parallel component, which can result in a heating of the electrons. This is the same type of process proposed by Norris et al [1983] to explain their dayside observations. (The electron observations of Norris et al were correlated to electromagnetic ion cyclotron waves, not electrostatic waves, however.) Conceptually, this is in contrast with the perpendicular acceleration implied by the observations of 'pancake' distributions at other times, in association with observations of electron Bernstein ($n + \frac{1}{2} f_{ce}$) waves (e.g. Wrenn et al [1979]; Olsen [1981]).

This process need not be very fast, since the electrons which we observe have presumably been drifting in the region between the plasmasphere and plasma sheet for many minutes, and perhaps hours. The

energization is low near the plasmasphere (damped?), and the energy density drops off at the plasma sheet as the plasma density drops.

The minimum in f, and subsequent region of positive slope at up to 1000 km/s, should allow for wave growth at that phase velocity. This would correspond to an electron energy of about 3 eV. Hence, waves in resonance with the region of positive slope would be able to interact with the core of the electron distribution function. There is a modest problem with this simple beginning - namely that the $k_{||}$ is much smaller than $k_{\perp}$. Hence, the parallel phase velocity will be much greater than the above noted value, and it may be that only the high-energy tail of the electron distribution can be heated. Of course, on day 95 enhancements in the parallel direction are seen up to almost 2 keV. For a 200 nT field, and assuming a density of ~100 /cm^3, with only H+ in the 'core' distribution, the Alfven velocity is 435 km/s. This is about 1 keV for protons, and well within the region of positive slope (see Figure 8).

The proton gyro frequency is about 3 Hz at this time. The 2-20 Hz band includes this value, or small multiples thereof. Jones et al [1981] reported some of the (relatively) rare observations of electrostatic waves at high altitudes, and with superior frequency resolution, were able to show they were banded emissions, with a frequency spacing of the order of the local He+ gyro frequency.

A frequency of 3 Hz, and a velocity of 1000 km/s implies a wavelength of ~300 km. This is substantially larger than the wavelength one might otherwise infer for cyclotron waves - e.g. the 50 km gyro radius of the hot protons. A slightly higher frequency, say 10 Hz, is still within the bounds of the data, and would give a wavelength closer to the gyro radius.

Modeling the transfer of energy from the high-energy ions, to the waves, and into the core plasma, is the obvious next step. Proposals to do so have not been funded. Some work has been done in this area, however, primarily looking at electromagnetic ion cyclotron waves. The most pertinent work appears to be a recent paper by Thorne and Horne [1992]. They model the generation of ion cyclotron waves in the outer plasmasphere, and show electron heating parallel to B. As Thorne and Horne suggest, the interactions illustrated here might explain some elements of electron precipitation, and the discrepancy between theory and observations vis-a-vis electron cyclotron waves and electron precipitation [Roeder and Koons, 1989].

Other possibilities exist. Hada et al [1981], whose observations in the tail bear remarkable similarity to these, discuss several alternatives. Fermi acceleration is one suggestion, but it seems inappropriate in the cases illustrated here, at substantially lower altitude.

The observation of electron distributions of high density and temperature at the convection boundary between the plasmasphere and plasma sheet is a new element in the collection of interactions between the hot and cold plasmas of the magnetosphere. Basic questions which naturally arise at this point revolve around the contrast between the transversely accelerated electrons which may also be observed around the plasmapause region, and the field-aligned electron distributions shown here. Under what circumstances do the contrasting processes occur? Since the energetic ion distributions, with their convection induced minima, are ubiquitous, it is most likely that differences have to do with the background electron density.

Acknowledgments

Sherman DeForest was the principal investigator for the UCSD particle detector. Carl McIlwain provided many of the resources at UCSD necessary to obtain the data. Tom Aggson was the principal investigator for the GSFC electric field experiment, Brian Ledley was the principal investigator for the GSFC magnetometer. Both have graciously provided access to the data, and substantial help in using the data. The suggestion to consider ion cyclotron waves as a means of heating electrons is due to Alain Roux, who patiently explained the concept several times over recent years. The analysis at NPS was supported by

NASA HQ under a grant, with computer facilities provided by NPS. Substantial use was made of the former NASA/SPAN network.

References

Chen, M. W., T. Hada, and M. Ashour-Abdalla, Ion-cyclotron wave heating of heavy ions in the equatorial magnetosphere: A numerical simulation study, in Modeling Magnetospheric Plasma, edited by T. E. Moore and J. H. Waite, pages 289-296, AGU, 1988.

Coates, A. J., A. D. Johnstone, J. J. Sojka, and G. L. Wrenn, Ionospheric photoelectrons observed in the magnetosphere at distances up to 7 earth radii, Planet. Space Sci, 1267-1275, 1985.

Comfort, R. H. and J. L. Horwitz, Low-energy ion pitch angle distributions on the day-side at geosynchronous altitudes, J. Geophys. Res., 86, 1621-1627, 1981.

Decreau, P. M. E., C. Beghin, and M. Parrot, Global characteristics of the cold plasma in the equatorial plasmapause region as deduced from the GEOS 1 mutual impedance probe, J. Geophys. Res., 87, 695-712, 1982.

DeForest, S. E., and C. E. Mcllwain, Plasma clouds in the magnetosphere, J. Geophys. Res., 76, 3587-3610, 1971.

Fennell, J. F., Description of P78-2 (SCATHA) satellite and experiments, in The IMS Source Book: Guide to the International Magnetospheric Study Data Analysis , edited by C. T. Russell and D. J. Southwood, 68-81, AGU, Washington DC, 1982.

Fennell, J. F., D. R. Croley, and S. M. Kaye, Low-energy ion pitch angle distributions in the outer magnetosphere: Ion zipper distributions, J. Geophys. Res., 86, 3375-3382, 1981.

Gough, M. P., P. J. Christiansen, G. Martelli, E. J. Gershuny, Interaction of electrostatic waves with warm electrons at the geomagnetic equator, Nature, 279, 515-517, 1979.

Greenspan, M. E., D. J. Williams, B. H. Mauk, and C.-I. Meng, Ion and electron energy dispersion features detected by ISEE-1, J. Geophys. Res., 90, 4079-4089, 1985.

Gurnett, D. A., Plasma wave interactions with energetic ions near the magnetic equator, J. Geophys. Res., 81, 2765-2770, 1976.

Hada, T., A. Nishida, T. Terasawa, and E. W. Hones, Bi-directional electron pitch angle anisotropy in the plasma sheet, J. Geophys. Res., 86, 11211-11224, 1981.

Horwitz, J. L., and C. R. Chappell, Observations of warm plasma in the dayside plasma trough at synchronous orbit, J. Geophys. Res., 84, 7075-7090, 1979.

Horwitz, J. L., R. H. Comfort, and C. R. Chappell, Thermal ion composition measurements of the formation of the new outer plasmasphere and double plasmapause during magnetic storm recovery, Geophys. Res. Left., 11, 701-704, 1984.

Johnson, J. F. E., J. J. Sojka, and G. L. Wrenn, Thermal/suprathermal plasmas observed by the S-302 experiment on GEOS-1, Space Science Rev, 22, 567-580, 1978.

Jones, D., A. Korth, K. Ronnmark, and D. Young, Helium cyclotron harmonic waves in the magnetospheric plasma, Adv. Space Res., 1, 319-324, 1981.

Kaye, S. M., E. G. Shelley, R. D. Sharp, and R. G. Johnson, Ion composition of zipper events, J. Geophys. Res., 86, 3383-3388, 1981.

Kivelson, M. G., S. M. Kaye, and D. J. Southwood, The Physics of Plasma Injection Events, in Dynamics of the Magnetosphere , edited by S.-I. Akasofu, D. Reidel, Dordrecht, Holland, 1979.

Kurth, W. S., J. D. Craven, L. A. Frank, and D. A. Gurnett, Intense electrostatic waves near the upper hybrid resonance frequency, J. Geophys. Res., 84, 4145-4164, 1979.

Laszakovits, J. S., Ionospheric photoelectrons measured at geosynchronous orbit, MS thesis, Naval Postgraduate School, Monterey, CA, June 1993.

Lennartsson, W, and D. L. Reasoner, Low-energy plasma observations at synchronous orbit, J. Geophys. Res., 13, 2145-2156, 1978.

Mauk, B. H., and R. L. McPherson, An experimental test of the electromagnetic ion cyclotron instability within the earth's magnetosphere, Phys. Fluids, 2 , 2111-2127, 1980.

Mcllwain, C. E., Plasma convection in the vicinity of the geosynchronous orbit, in Earth's Magnetospheric Processes, edited by B. M. McCormac, pages 268-279, D. Reidel Publishing Company, Dordrecht-Holland, 1972.

Mcllwain C. E., Auroral electron beams near the magnetic equator, in Physics of the Hot Plasma in the Magnetosphere, Plenum, 1975.

Mcllwain, C. E. , and E. C. Whipple, The dynamic behavior of plasmas observed near geosynchronous orbit, IEEE Trans. Plasma Sci., PS-14, 874-890, 1986

Moore, T. E., and R. L. Arnoldy, Plasma pitch angle distributions near the substorm injection front, J. Geophys. Res., 87, 265-270, 1982.

Norris, A. J., J. F. E. Johnson, J. J. Sojka, G. L. Wrenn, N. Cornilleau-Wehrlin, S. Perraut, and A. Roux, Experimental evidence for the acceleration of thermal electrons by ion cyclotron waves in the magnetosphere, J. Geophys. Res,, $$, 889-898, 1983.

Olsen, R. C., Equatorially trapped plasma populations, J. Geophys. Res., $f, 11235-11245, 1981.

Olsen, R. C., The hidden ion population of the magnetosphere, J. Geophys. Res., $Z, 3481-3488, 1982.

Olsen, R. C., S. D. Shawhan, D. L. Gallagher, J. L. Green, and C. R. Chappell, Plasma observations at the earth's magnetic equator, J. Geophys. Res., 92, 2385-2407, 1987.

Olsen, R. C., and C. W. Norwood, Spacecraft-generated ions, J. Geophys. Res., 15951-15962, 1991.

Omura, Y., M. Ashour-Abdalla, R. Gendrin, and K. Quest, Heating of thermal helium in the equatorial magnetosphere: A simulation study, J. Geophys. Res., 90, 8281-8292, 1985.

Perraut, S., A. Roux, P. Robert, R. Gendrin, J.-A. Sauvaud, J.-M. Bosqued, G. Kremser, and A. Korth, A systematic study of ULF waves above FH+ from GEOS 1 and 2, measurements and their relationships with proton ring distributions, J. Geophys. Res., 82, 6219-6236, 1982.

Quinn, J. M. and R. G. Johnson, Observation of ionospheric source cone enhancements at the substorm injection boundary, J. Geophys. Res,., 90, 4211-4220, 1985.

Roeder, J. L. and H. C. Koons, A survey of electron cyclotron waves in the magneto-sphere and the diffuse auroral electron precipitation, J. Geophys. Res., 94, 2529-2541, 1989.

Roux, A., S. Perraut, J. L. Rauch, C. de Villedary, G. Kremser, A. Korth, and D. T. Young, Wave-particle interactions near the helium gyrofrequency observed on GEOS 1 and 2, 1. Generation of ion cyclotron waves and heating of He+ ions, J. Geophys. Res., 87, 8174-8190, 1982.

Russell, C. T., R. E. Holzer, and E. J. Smith, OGO 3 observations of ELF noise in the magnetosphere, 2. The nature of the equatorial noise, J, Geophys. Res., 75, 755-768, 1970.

Scott, L. J., On the consequences of bi-Maxwellian distributions on parallel electric fields, M.S. thesis, Naval Postgraduate School, 1991.

Serbu, G. P., E. J. R. Maier, Low energy electrons measured on IMP 2, J. Geophys. Res., 71, 3755-3766, 1966.

Singh, N. Refilling of a plasmasphere flux tube - Microscopic plasma processes, Modeling Magnetospheric Plasma, Geophysical Monograph 44, edited by T. E. Moore and J. H. Waite, published by American Geophysical Union, Washington D. C., pages 87-99, 1988.

Sojka, J. J., G. L. Wrenn, and J. F. E. Johnson, Pitch angle properties of magnetospheric thermal protons and satellite sheath interference in their observation, J. Geophys. Res., 89, 9801-9811, 1984.

Sojka, J. J., and G. L. Wrenn, Refilling of geosynchronous flux tubes as observed at the equator by GEOS 2, J. Geophys. Res., 90, 6379-6385, 1985.

Thorne, R. M., and R. B. Horne, The contribution of ion-cyclotron waves to electron heating and SAR-arc excitation near the storm-time plasmapause, Geophys. Res. Lett., 19, 417-420, 1992

Young, D. T., S. Perraut, A. Roux, C. de Villedary, R. Gendrin, A. Korth, G. Kremser, and D. Jones, Wave-particle interactions near the helium gyrofrequency observed on GEOS 1 and 2, 1. Propagation of ion cyclotron waves in He+ rich plasma, J. Geophys. Res., 86, 6755-6772, 1981.

Wrenn, G. L., J. F. E. Johnson, and J. J. Sojka, Stable 'pancake' distributions of low energy electrons in the plasma trough, Nature, 279, 512-514, 1979.